Malvinas Current variability from Argo floats and satellite altimetry

Camila Artana, Ramiro Ferrari, Zoé Koenig, Martin Saraceno, Alberto R. Piola, Christine Provost

AGU PUBLICATIONS

JGR

Journal of Geophysical Research: Oceans

RESEARCH ARTICLE

10.1002/2016JC011889

Key Points:
- Blocking events at around 48.5°S, coupled to SSH variation, are a recurrent feature of the MC circulation
- The Malvinas Plateau, where energetic deep-reaching eddies are trapped, break down, and vanish, appears as a hot spot for dissipation
- SLA across the NSR do not impact the MC further north except for coastal trapped waves that propagate through EBB

Correspondence to:
C. Artana,
cartlod@locean-ipsl.upmc.fr

Citation:
Artana, C., R. Ferrari, Z. Koenig, M. Saraceno, A. R. Piola, and C. Provost (2016), Malvinas Current variability from Argo floats and satellite altimetry, *J. Geophys. Res. Oceans*, *121*, 4854–4872, doi:10.1002/2016JC011889.

Received 15 APR 2016
Accepted 7 JUN 2016
Accepted article online 9 JUN 2016
Published online 16 JUL 2016

Malvinas Current variability from Argo floats and satellite altimetry

Camila Artana[1], Ramiro Ferrari[2], Zoé Koenig[1], Martin Saraceno[3], Alberto R. Piola[4], and Christine Provost[1]

[1]Laboratoire LOCEAN-IPSL, Sorbonne Universités, UPMC, Univ. Paris 6-CNRS-IRD-MNHN, Paris, France, [2]CIMA/CONICET-UBA and UMI IFAECI-3351, Buenos Aires, Argentina, [3]CIMA/CONICET-UBA DCAO/FCEN/UBA and UMI-IFAECI 3351, Buenos Aires, Argentina, [4]Departamento de Oceanografía, Servicio de Hidrografía Naval, DCAO/FCEN/UBA and UMI-IFAECI 3351, CONICET, Buenos Aires, Argentina

Abstract The Malvinas Current (MC) is an offshoot of the Antarctic Circumpolar Current (ACC). Downstream of Drake Passage, the northern fronts of the ACC veer northward, cross over the North Scotia Ridge (NSR) and the Malvinas Plateau, and enter the Argentine Basin. We investigate the variations of the MC circulation between the NSR and 41°S and their possible relations with the ACC circulation using data from Argo floats and satellite altimetry. The data depict meandering and eddy shedding of the northern ACC jets as they cross the NSR. The altimetry fields show that these eddies are trapped, break down, and dissipate over the Malvinas Plateau, suggesting that this region is a hot spot for dissipation of mesoscale variability. Variations of sea level anomalies (SLA) across the NSR do not impact the MC further north, except for intra-seasonal variability associated with coastal trapped waves. Altimetry and float trajectories show events during which a large fraction of the MC is cut off from the ACC. Blocking events at around 48.5°S are a recurrent feature of the MC circulation. Over the 23 year altimetry record, we detected 26 events during which the MC surface transport at 48.5°S was reduced to less than half its long-term mean. Blocking events last from 10 to 35 days and do not present any significant trend. These events were tracked back to positive SLA that built up over the Argentine Abyssal Plain. Future work is needed to understand the processes responsible for these blocking events.

1. Introduction

The persistent westerly winds over the Southern Ocean drive the Antarctic Circumpolar Current (ACC) flow around the Antarctic continent. The ACC flow is organized in three oceanic frontal systems, which correspond to water mass boundaries as well as deep-reaching jets of eastward flow: the Subantarctic Front (SAF), the Polar Front (PF), and the Southern ACC Front (SACCF) [*Nowlin et al*., 1977; *Orsi et al*., 1995]. These narrow fronts are themselves composed of distinct branches that meander, split, merge, and spinoff eddies [*Sokolov and Rintoul*, 2009a, 2009b].

In Drake Passage, *Barré et al*. [2011] identified the multiple branches associated with the ACC fronts (SAF-N, SAF-M, PF-N, PF-M, PF-S, SACCF-N, and SACCF-S) in the sea surface topography (Table 1) and observed that the branch locations were steered by bottom topography (Figure 1a). Downstream of Drake Passage, the Scotia Arc forms a large topographical obstacle to the ACC flow. The North Scotia Ridge (NSR), the South Sandwich Island Arc, and the South Scotia Ridge force the ACC to flow through relatively narrow passages. The northern part of the ACC (e.g., the flow associated with the SAF and PF) veers to the north crossing the NSR through narrow passages: the SAF-N proceeds through a sill to the West of Burwood Bank (WBB), the SAF-M through a sill to the East of Burwood Bank (EBB), and the PF branches through Shag Rocks Passage (SRP) (Figure 1a). The SACCF branches follow eastward paths south of South Georgia. After crossing the North Scotia Ridge and the Malvinas Plateau, the SAF follows the western slope of the Argentine Basin to form the Malvinas Current, whereas the PF follows an eastward path along the southern edge of the Argentine Basin at 50°S (Figure 1b).

The Malvinas Current (MC) is thus an offshoot of the northern part of the ACC. This deep-reaching current carries the cold (<7°C at the surface in winter) and relatively fresh Subantarctic Water equatorward

Table 1. ADT Values Associated With ACC Fronts[a]

Fronts	ADT (m)
SAF-N	0.23
SAF-M	−0.10
PF-N	−0.43
PF-M	−0.62
PF-S	−0.79
SACCF-N	−0.93
SACCF-S	−1.14

[a]From *Barré et al.* [2011].

following the 1000–2000 m isobaths along the Patagonian shelf break [*Piola and Gordon*, 1989], until it meets the Brazil Current (BC) at around 38°S (Figure 1b). The meeting of the MC and the BC is known as the Brazil-Malvinas Confluence. After they meet, both currents separate from the continental slope and turn offshore [*Gordon*, 1989]. The MC retroflects cyclonically southward: the SAF undergoes a sharp loop toward the south and joins the southern edge of the Argentine Basin at 49°S 49°W, nearly merging with the PF and creating an intense eastward flow. Part of the Brazil Current, referred to as the overshoot of the Brazil Current, flows southward and returns to the northeast at about 45°S [*Saraceno et al.*, 2004]. Another important feature of the circulation in the southwest Atlantic is the Zapiola anticyclone, a 1500 km diameter feature centered at 45°W–45°S over a sediment deposit in the Argentine Basin, with a volume transport comparable to those of the major ocean current (80 Sv) [*Saunders and King*, 1995; *Fu*, 2006; *Volkov and Fu*, 2008; *Saraceno et al.*, 2009].

While the Brazil-Malvinas Confluence and the retroflection region are amongst the most energetic regions of the world ocean [e.g., *Chelton et al.*, 1990] with eddy kinetic energy reaching values in excess of 2000 $cm^2\ s^{-2}$, the Malvinas Current and Zapiola region show relatively low eddy kinetic energy levels ($<$300 $cm^2\ s^{-2}$) (Figure 1c).

The lack of correlation between the northward penetration of the MC and wind forced pulses of the ACC [e.g., *Garzoli and Giulivi*, 1994] suggest that the MC variations are uncoupled from the ACC. This is also suggested by the analysis of numerical simulations, which suggest that locally generated high-frequency anomalies mask the connection between the variability of the ACC and that of the MC [*Fetter and Matano*, 2008]. The variability of the Malvinas Current has been monitored at 41°S near its merger with the BC with current meter moorings and satellite altimetry [*Vivier and Provost*, 1999a, 1999b; *Spadone and Provost*, 2009]. Variability with a periodicity of about 70 days is coherent with bottom-pressure variability on the northern side of Drake Passage with a time lag shorter than 20 days. This variability is associated with a baroclinic shelf wave propagating along the edge of the Patagonian Shelf at a speed of 2.5–3 $m\ s^{-1}$ [*Vivier et al.*, 2001]. Variations near the semiannual period appear to reflect barotropic adjustment to changes in the wind stress curl north of 50°S in the Pacific Sector [*Vivier et al.*, 2001]. However, the location of the moorings just upstream of the confluence with the BC made it difficult to distinguish variations with a southern origin from mesoscale variations due to the proximity of the Brazil-Malvinas Confluence. There are no direct current observations in the MC further south and its variability south of 41°S has received little attention.

In Drake Passage, the southern flank of the NSR is the site of local maxima in EKE (values reaching 1000 $cm^2\ s^{-2}$) associated with the SAF and PF (Figure 1c). The decrease in EKE on the northern side of the ridge is due to the influence of the NSR, a topographic barrier reducing eddy activity. Values south of the NSR are at least a factor of two to three higher than those to the north. High EKE seems to leak across the ridge in the vicinity of the EBB and SRP. *Fetter and Matano* [2008], using an eddy-permitting ocean general circulation model (18 years, 1/4° grid spacing, 20 vertical levels), showed the existence of a mode in the ACC transport at Drake Passage with a 150 day period, that generates out-of-phase changes in the transport crossing NSR through EBB and through SRP. The impacts of these variations in the crossing of the NSR on the Malvinas Current were rather inconclusive, due to the low-resolution model producing a Malvinas Current with an unrealistic short meridional extent.

This work investigates variations in the circulation of the MC as they are documented by 14 years of Argo float data and 23 years of satellite altimetry. Argo float data reveal interesting behaviors as shown in four examples of trajectories in Figure 1d: a float in the MC that crossed NSR through SRP and not through EBB as expected (in dark blue), a float in the MC that crossed NSR through EBB and never managed to proceed north of 45°S (light blue), a float that crossed NSR through SRP joined the MC and is blocked south of 49°S (in red) and a float that goes through EBB and is trapped in eddies just north of NSR over the Malvinas Trough and then over the Malvinas Plateau (in green). These trajectories suggest that the link between the

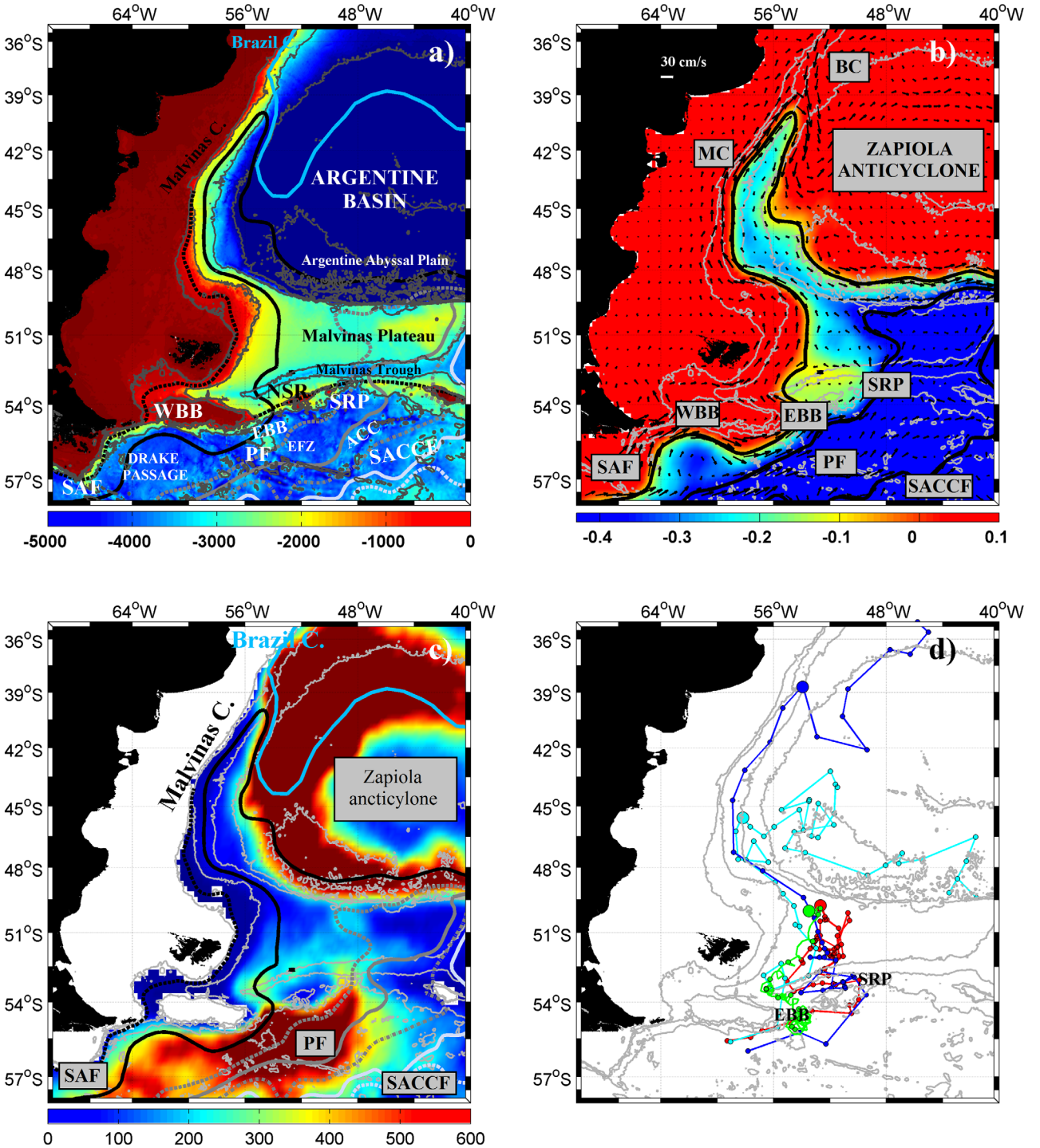

Figure 1. (a) Bottom topography of the Southwestern Atlantic and Drake Passage (in meters) from *Smith and Sandwell* [1994]. The 6000, 5000, 3000 1000, and 300 m isobaths are represented with solid light grey contours. The ridge associated with the Endurance Fracture Zone (EFZ) at the exit from Drake Passage is labeled. The main passages through North Scotia Ridge (NSR) are indicated: West of Burwood Bank (WBB), East of Burwood Bank (EBB), and Shag Rocks Passage (SRP). A black dashed line follows the crest of the NSR. The mean location of the main Antarctic Circumpolar Current (ACC) fronts as defined by *Barré et al.* [2011] are plotted: Subantarctic Front (SAF), in black (SAF-M solid line and SAF-N dashed line); Polar Front (PF), in dark grey (PF-M solid line and PF-N and PF-S dashed line); and Southern ACC Front (SACCF), in light grey (SACCF-S dashed line and SACCF-N solid line). The mean position of the Brazil Current Front (BCF, solid light blue line) is from *Saraceno et al.* [2004]. (b) Mean absolute dynamic topography (in meters) and corresponding surface geostrophic velocities (cm/s) derived from 23 years (1993–2015) of satellite altimeter data. The mean location of the ACC fronts and the isobaths are as in Figure 1a. (c) EKE values (cm^2/s^2) for the same period as Figure 1b estimated from satellite altimetry data from the geostrophic currents. The fronts and isobaths are as in Figure 1a. (d) Trajectories of Argo floats 5901852, 3900424, 3900085, and 6901650 represented by dark blue, light blue, red dotted line, and green dotted line, respectively. In each trajectory, the large color dot represents the northernmost location of the float in the MC. Grey lines represent the same isobaths that in Figure 1a.

Table 2. Potential Density Values at 400 db Associated With the Main ACC Fronts

Fronts	Potential Density at 400 db
North SAF	$\sigma < 27.15$
SAF-PF	$27.15 < \sigma < 27.48$
PF-SACCF	$27.48 < \sigma < 27.65$
South SACCF	$\sigma > 27.65$

ACC and the MC at times may not be straightforward. We investigate here why these particular floats do not continue their northward path, as expected for particles trapped in the MC.

We proceed from the South and first examine the variations of the ACC fronts as they cross the North Scotia Ridge. We describe sea level anomalies with respect to the mean, the fate of the anomalies over the shallow Malvinas Plateau and their impact on the Malvinas Current. Then we proceed northward examining variations along the slope of the western edge of the Argentine Basin.

The paper is organized as follows. In section 2, Argo float and satellite altimetry data are used to describe the mean location and the variations of the northern ACC fronts across the North Scotia Ridge and to analyze the impacts of these variations on the Malvinas Current. Section 3 examines variations along the continental slope and documents large blocking events that occasionally disconnect the Malvinas Current from its southern source. Finally, section 4 synthesizes the main results of this study and puts forward several perspectives.

2. The ACC Across the North Scotia Ridge and Malvinas Plateau

Daily maps of absolute dynamic topography (ADT), surface geostrophic velocities, and sea level anomalies (SLA) for the period 1993–2015 were used in this study (total of 8400 maps). These gridded maps with a grid spacing of 1/4° were produced by Ssalto/Duacs and distributed by AVISO (http://www.aviso.oceanobs.com).

Argo float data (http://www.usgodae.org) from 2002 to 2015 were also considered. The Argo floats drift at 2000 db (parking depth) and they provide temperature and salinity profiles between 0 and 2000 db with a typical vertical resolution of 10 db every 10 days.

2.1. Mean Location of the ACC Across North Scotia Ridge

The three ACC fronts correspond to large gradients in potential density at 400 db. Consequently, potential density at 400 db is a good indicator of the location of a hydrographic profile relative to the ACC fronts (Table 2) [*Provost et al*., 2011]. Argo float profiles (9160 profiles over 2002–2015) were classified based on their potential density at 400 db (Figure 2a). Profile locations are presented on the same map while they were taken during 14 years and in all seasons. Different colors in the same location indicate eddies or frontal meanders. The location of fronts inferred from Argo float data and the mean location of fronts deduced from altimetry using the absolute dynamic topography criteria defined in *Barré et al*. [2011] (Table 1) are in good agreement (Figure 2a). However, in contrast with the altimetry-derived fronts, Argo float data show the occurrence of north of SAF waters, i.e., Subantarctic Waters, in the SRP (blue dots in Figure 2a) and of south of PF waters, i.e., Antarctic waters, in the EBB (green dots in Figure 2a), indicating sporadic meandering of fronts or eddies through these passages (Figure 2a). Moreover, Temperature-Salinity diagrams corresponding to the 359 and 376 profiles present in the EBB and SRP areas (delimited by the boxes indicated in Figure 2a) confirm the presence of Subantarctic Waters in the SRP, and Antarctic Waters in the EBB (Figures 2b and 2c). Indeed, the density at 400 db (colored dots in Figures 2b and 2c) further indicates that waters from north of the SAF are found in the SRP in 34 profiles (blue dots with density lower than 27.15 kg/m^3 in Figure 2c), and, that waters from south of the PF are found in EBB in 7 profiles (green dots with density larger than 27.48 kg/m^3 in Figure 2b).We made use of the full altimetry record from the archiving, validation and interpretation of satellite oceanographic data (AVISO, www.aviso.oceanobs.com) to evaluate the time-space variability of the SAF and PF in the NSR. For this purpose, all time series are detrended by subtracting the record-length linear trend in SLA.

2.2. Variations of the ACC Across North Scotia Ridge Based on Satellite Altimetry

We analyze the time variability of absolute dynamic topography (ADT) from 1993 to 2015 along a section following the NSR crest between 55°W and 44°W (dash black line Figure 1a). High values (>-10 cm) are associated with the position of the SAF-M (Figure 3) while the position of the PF corresponds to the values between -43 and -79 cm [*Barré et al*., 2011]. The time-mean SAF-M crosses the NSR through the EBB and

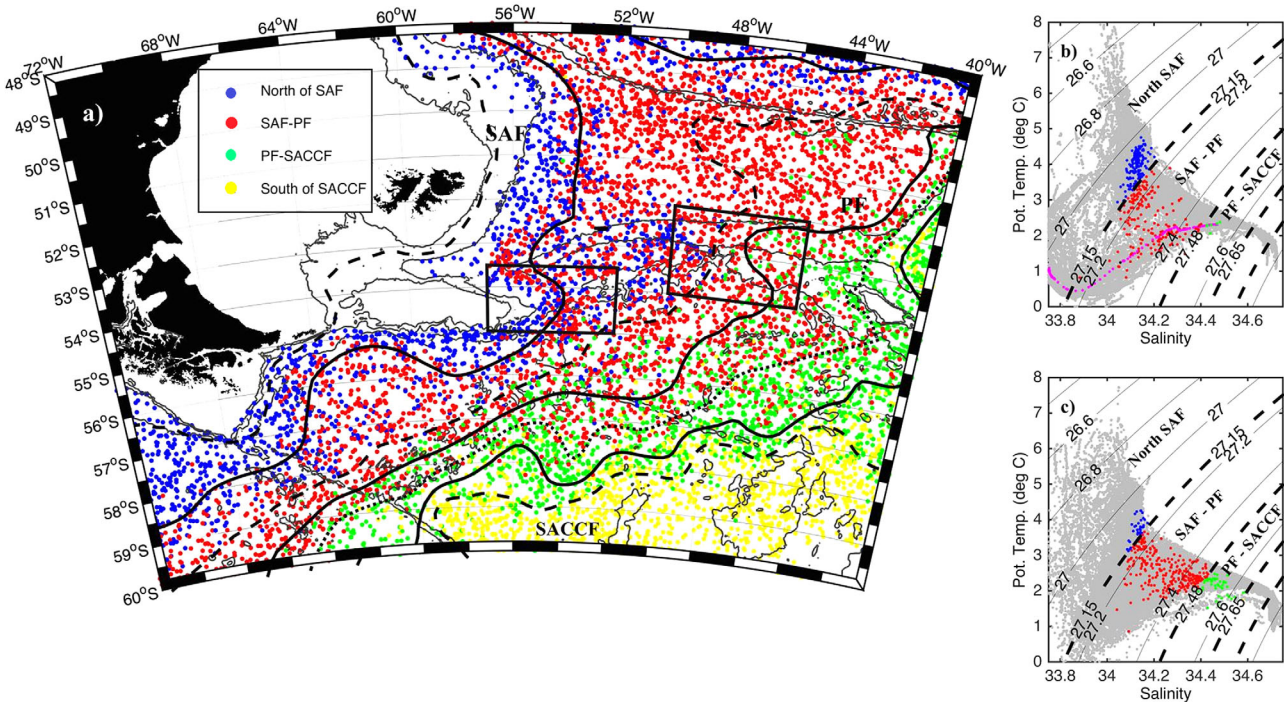

Figure 2. (a) Argo float profiles (9160 profiles over 2002–2015) classified based on their potential density at 400 dbars. North of SAF are labeled in blue; SAF-PF in red; PF-SACCF in green; and south of SACCF in yellow. The main ACC fronts are indicated as in Figure 1a. (b) Potential temperature-Salinity diagram corresponding to the 359 profiles from the floats that crossed through the domain over EBB limited by the black box in Figure 2a. All the profiles are in grey with the values at 400 db in colour. The black dashed line corresponds to the density separation between SAF, PF, and SACCF (Table 2). The magenta profile corresponds to float 6901650 (green on Figure 1d) on 14 June 2015. (c) same as Figure 2b over SRP (black box in Figure 2a). On the figure, 376 profiles are plotted.

the time-mean PF through the SRP. However, the highly variable SAF-M positions reach as far east as 49°W suggesting sporadic migrations of the SAF-M to the SRP (Figure 3). Similarly, ADT values within the PF range are observed near 54°W in the EBB. ADT values larger than −10 cm were found 63 times in 8400 maps at 49.2°W in SRP. A spectral analysis of the ADT time series at 49.2°W in SRP (not shown) presented a significant peak at 150 days, reminiscent of the dominant spectral peak in the model transport variability seen by *Fetter and Matano* [2008]. ADT values lower than −43 cm were observed 39 times in EBB.

2.3. Extrema and Selected Cases

Mean surface geostrophic velocity fields for the altimetric time series (mean over 8400 maps), and composites during events when ADT is larger than −10 cm at 49.2°W (composite of 63 cases), and when ADT is lower than −43 cm at EBB (composite of 39 cases) are shown in Figures 4a–4c. These velocity fields suggest that SAF-M undergoes a 300 km eastward overshoot crossing the NSR over the SRP and the PF meanders westward toward the EBB, though without fully crossing it (Figures 4a–4c). Mean surface velocity sections along the NSR crest show that the eastward migrations of the SAF through SRP lead to increased surface velocities in excess of 40 cm/s at 49°W whereas PF displacements toward the EBB lead to surface velocities in excess of 50 cm/s at EBB (Figure 4d).

Examination of the ADT map time series shows that the PF shed eddies through EBB, while there is no evidence of it meandering through the EBB. The eddies often migrated to the northwest and remained for some time (about 8 weeks) trapped in the Malvinas Trough at 54.5°W and 54°S. As an example, the ADT evolution in May–August 2015 is presented (Figure 5). After crossing the NSR through the EBB, and being trapped in the Malvinas Trough for 8 weeks, a 100 km diameter eddy managed to proceed northward up onto the Malvinas Plateau where it broke apart after 2 weeks. An exceptionally clear 1 km resolution MODIS sea surface temperature image shows the eddy broken into two smaller eddies (radii of about 50 km located around 55°W and 52°S) tied to each other by a filament (Figure 5h). At that time, the amplitude of the altimetry signal decreases and it is not possible to further track the eddy (Figure 5g). An Argo float programmed to collect daily profiles down to 1000 m, trapped in the eddy from 7 May to 8 August, documents

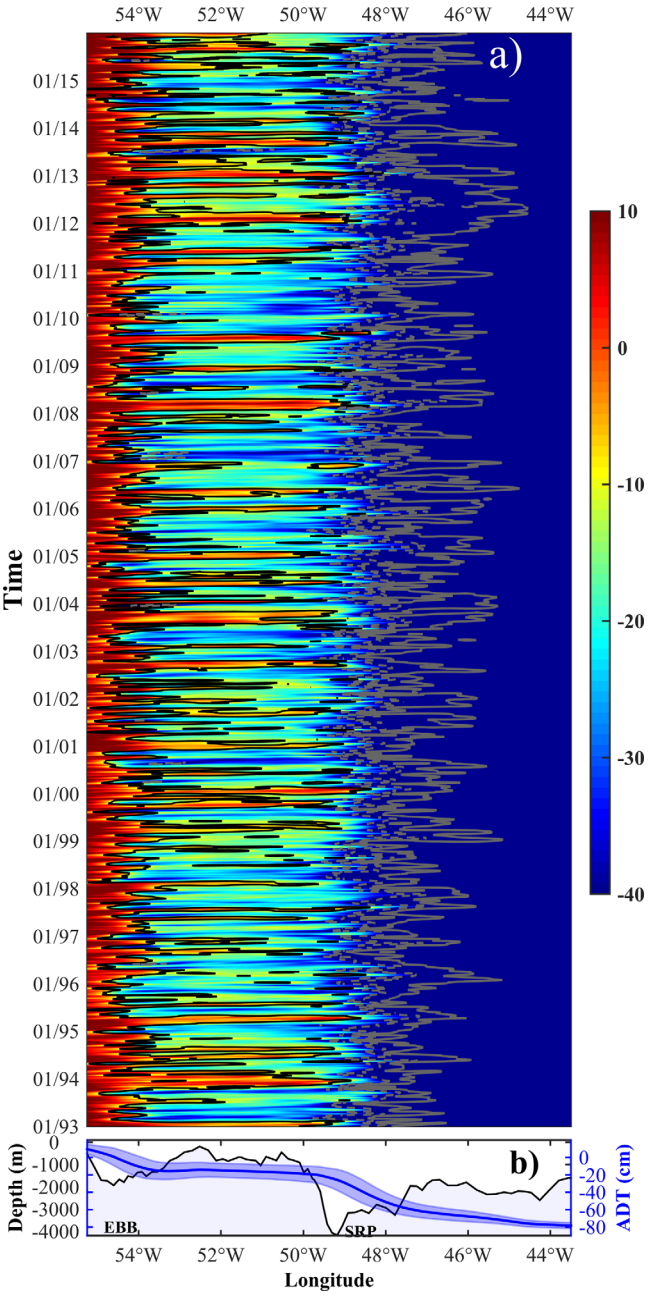

Figure 3. (a) Hovmöller diagram of Absolute Dynamic topography (ADT) between 1993 and 2015 along the NSR transect shown in Figure 1a. Location of the SAF (in black) and PF (in grey) according to the corresponding ADT values in Table 1. (b) Bathymetry (black line), mean, and standard deviation of absolute dynamic topography (blue line, shaded blue) along the NSR transect.

its thermohaline structure, displacement velocity and its disintegration (Figure 6). Initially the 100 km diameter eddy makes a complete rotation in 4–5 days, which implies a tangential velocity on the order of 1 m s^{-1}. The minimum temperature at 200 m, close to 0°C, and the low-salinity values (less than 33.8 psu) (see also magenta profile in Figure 2b), correspond to the typical winter water characteristics from south of the PF, corroborating that from early May to early August the float is trapped in a cold core eddy of southern origin. In early August, float 6901650 undergoes a dramatic change in thermohaline properties that extends throughout the upper 1000 m. The subsurface temperature minimum at around 200 m is replaced by relatively warm (~3.5 to 4.5°C) temperatures extending over the upper 600 m of the water column (Figure 6). Simultaneously the salinity increases from 33.8 to 34.1 psu in the upper layer. The ADT distribution from August 8 (Figure 5g) clearly indicates that the sharp change observed in the waters sampled by float 6901650 are associated with the dissipation of the eddy, and not to the float displacement across the eddy rim and into surrounding Polar Front waters. The strong deep-reaching (>1000 m) and large (>100 km) eddy disappears from the ADT maps in about 3 months (May–August) over the Malvinas Plateau (Figure 5). It is important to recall that only eddies with radii larger than 50 km can be tracked in ADT maps with the present satellite altimetry coverage. The precise fate of the pair of small eddies remains undetermined as clear high-resolution sea-surface temperature images in this region are exceptional due to the usual dense cloud cover.

Examination of the ADT map time series also shows that the SAF either meanders through the SRP or sheds anticyclonic eddies that cross the NSR through the SRP. A SAF meander over the SRP may last a few weeks as for example in March 2008. When the SAF retreats back east, an anticyclonic eddy is shed (not shown). Anticyclonic eddies are observed in the Malvinas Trough and on the Malvinas Plateau, often travel west along the Malvinas Trough and end up recoalescing with the SAF (not shown). This preferred path contributes to the local maximum in EKE (>200 cm^2 s^{-2}) over the Malvinas Trough (Figure 1c).

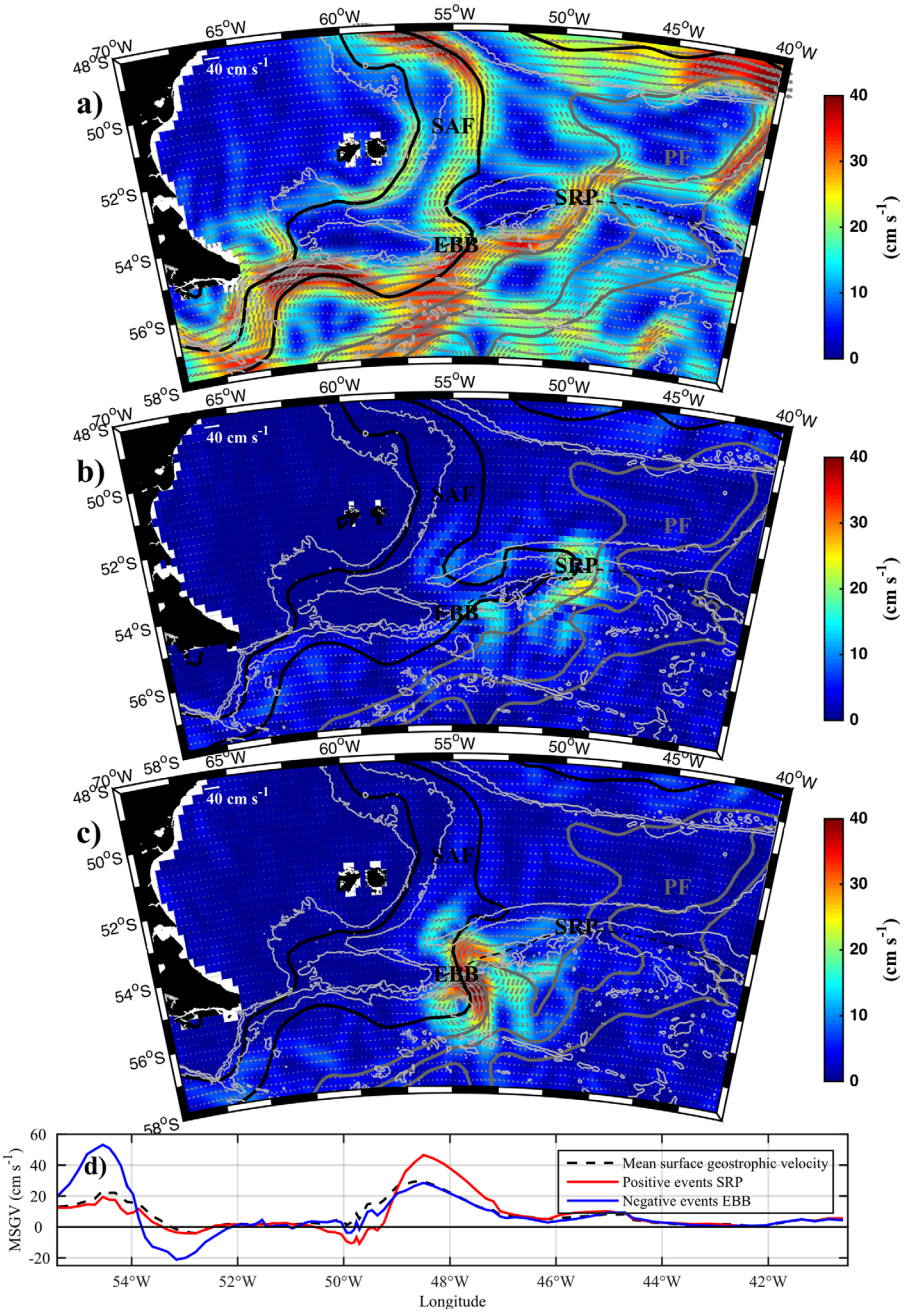

Figure 4. (a) Location of the SAF (black) and PF (grey) as defined by *Barré et al.* [2011] superimposed on direction (vectors) and intensity (colors) of the mean surface geostrophic velocities for 1993–2015 period. (b) Mean location of SAF (black) and PF (grey) while the SAF-M flows through SRP superimposed on velocities anomalies relative to the mean. (c) Mean location of SAF (black) and PF (grey) while the PF-N flows through EBB superimposed on velocities anomalies relative to the mean. (d) Mean surface velocity sections along the NSR crest for the altimetric time series (dashed line), for the events from Figure 4c (blue line) and for those from Figure 4b (red line).

2.4. Impact of the Variations Across NSR on the MC

In order to document the origin and impact of the SLA variations at EBB (and SRP), the time series of SLA over a box centered at EBB (and SRP) was regressed onto SLA fields at several time lags. Selected lagged regression maps of SLA onto the SLA time series at EBB and at SRP are shown in Figures 7a and 7b, respectively. Significant regressions (above the 95 or 99% confidence level) are observed over a wide range of lags (from −50 to + 80 days for EBB and from −70 to + 110 days for SRP) and display different features. Regression maps onto EBB (Figure 7a) show significant patterns along the slope that are probably associated with

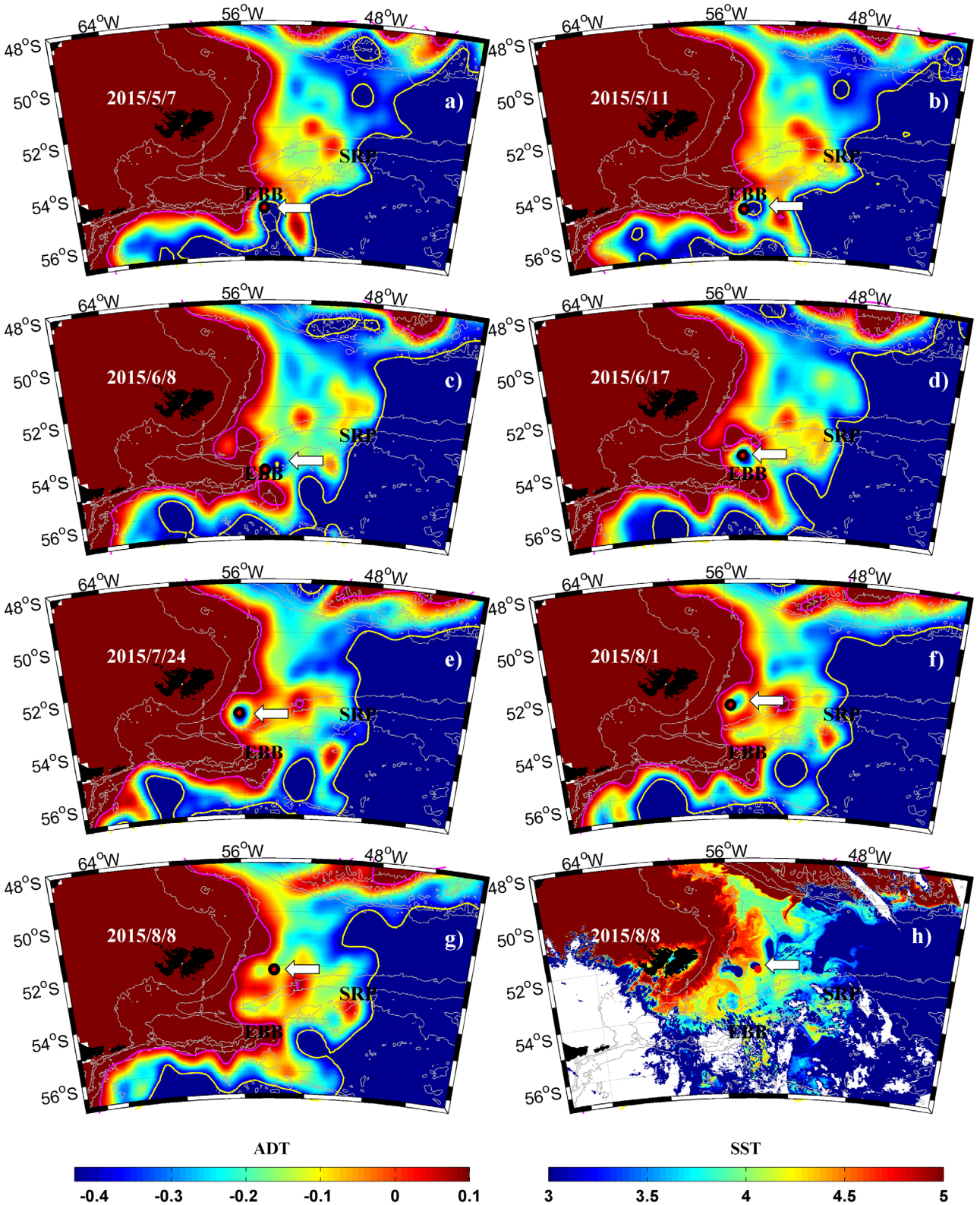

Figure 5. (a–g) Selected ADT maps from May to August 2015 as an example of the PF shedding a cyclonic eddy through EBB. (h) High-resolution SST image from MODIS for the date corresponding to the 8 August 2015 (same as Figure 5g). The position of the eddy is indicated with a white arrow, and the red dot indicates the position of Argo float 6901650. Color scale for ADT is in meter, color scale for SST in degree Celsius. The SAF and PF locations as defined by *Barré et al.* [2011] are represented by magenta and yellow contours, respectively. Isobaths are the same as in Figure 1a.

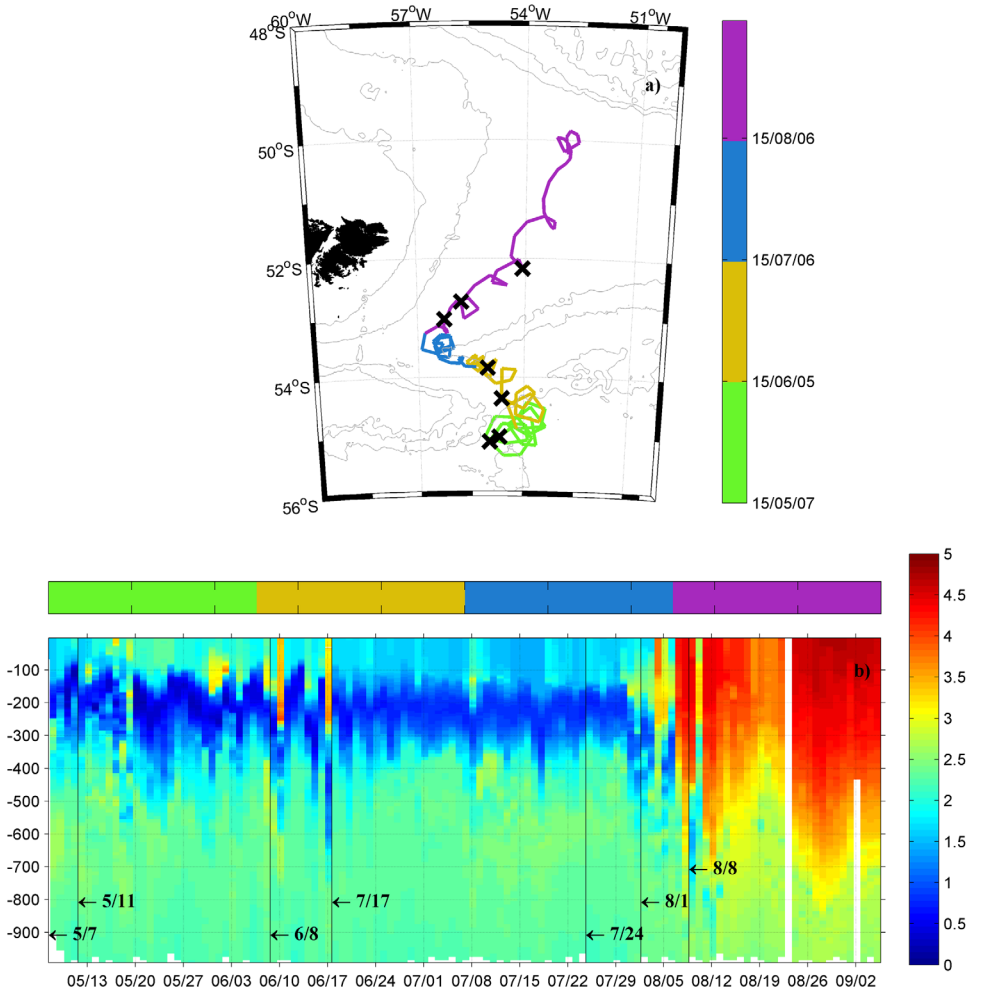

Figure 6. (a) Trajectory of Argo float 6901650 in different colors to distinguish time periods. (b) Potential temperature profiles from the Argo float (daily resolution). Black crosses in Figure 6a and vertical lines in Figure 6b indicate the position and the dates shown in each plot of Figure 5.

fast baroclinic coastal trapped waves propagating along the edge of the Patagonian Shelf [*Vivier et al.*, 2001]. The rapid propagation speed of these waves, on the order of a few m s^{-1}, is not resolved in the altimetry maps [*Koenig et al.*, 2016]. In contrast, regression maps with SRP do not show significant correlations along the continental slope at lags shorter than 110 days (Figure 7b).

At negative lags starting at −50 days for EBB and −70 days for SRP, regression maps show tripole or dipole mesoscale SLA patches slowly progressing eastward and building up in amplitude as they are blocked by the topography (Endurance Fracture Zone, EFZ indicated in Figure 1a and NSR). Significant anomalies at lag 0 have amplitudes in excess of 10 cm.

As the anomaly crosses the NSR, it spreads in longitude trapped along the relatively deep Malvinas Trough (>3000 m) for about 50 days and then proceeds northward onto the shallow (<3000 m) Malvinas Plateau where its breaks up and decreases in amplitude. There are no significant correlations over the Malvinas Plateau at lags > 80 days in the regression maps onto EBB nor at lags > 110 days in the regression maps onto SRP.

This regression analysis suggests that the anomalies observed at EBB and SRP build up around the EFZ in a similar way, those reaching SRP being of larger amplitude. The fate of the SLA anomalies after they flow over the NSR, whether observed at EBB or SRP are quite similar: they are first trapped in the Malvinas Trough and then break up as they proceed northward over the Malvinas Plateau. They are no longer observed in altimetry maps.

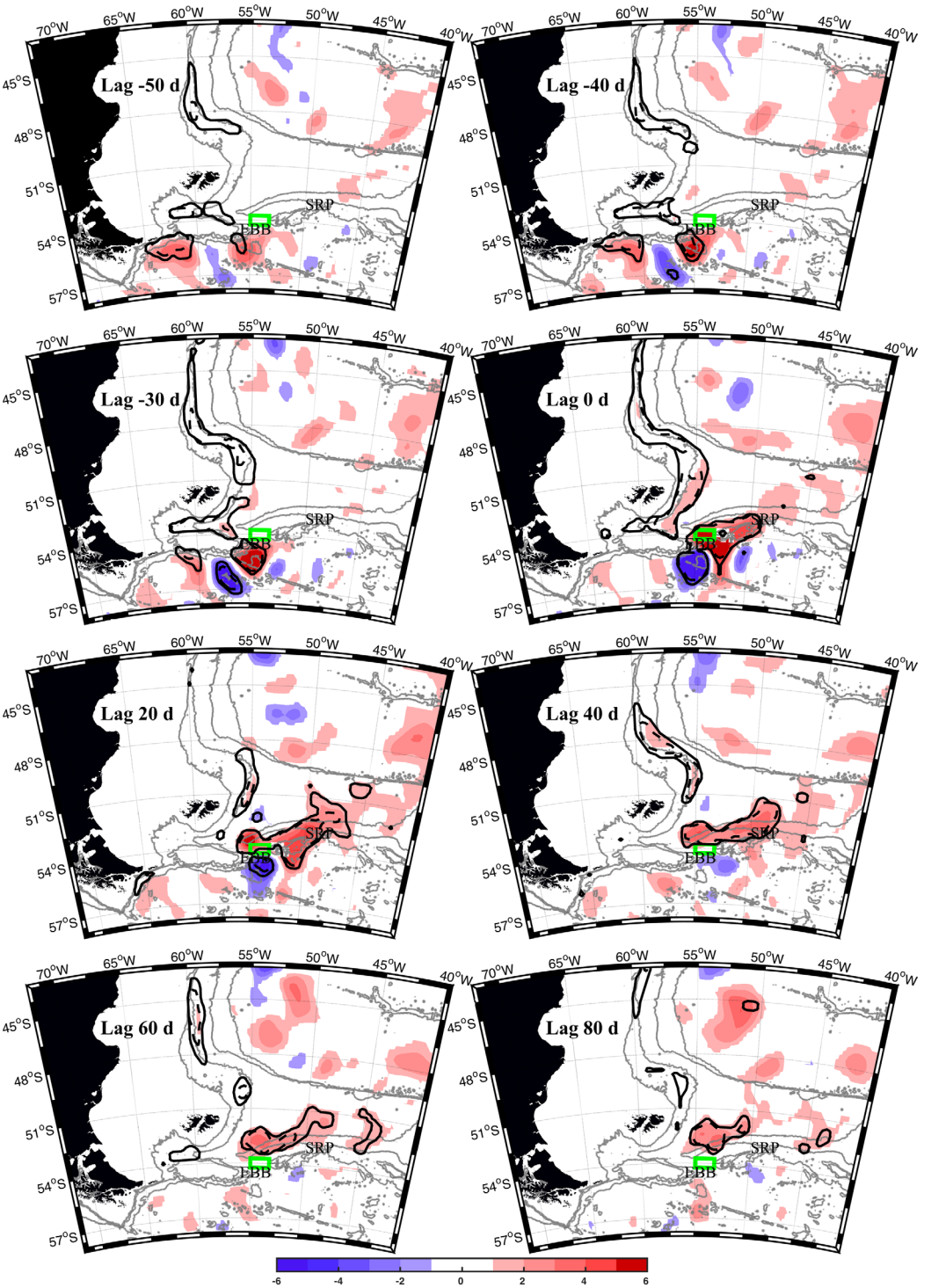

Figure 7. (a) Regression of SLA on the normalized time series of SLA at EBB box (green box). Solid black contours represent the correlation at the 90% confidence level; dashed black contours represent the 95% confidence level. Color scale is SLA in centimeter. Bathymetry is shown with grey contours at 5000, 3000, 1000, and 300 m.

The SLA time series at EBB and SRP are significantly correlated with a maximum correlation coefficient of 0.4 at a 25 days lag, with EBB leading SRP. Indeed, the SLA regression map onto EBB at lag −30 days is quite similar to the SLA regression map onto SRP at lag −70 days.

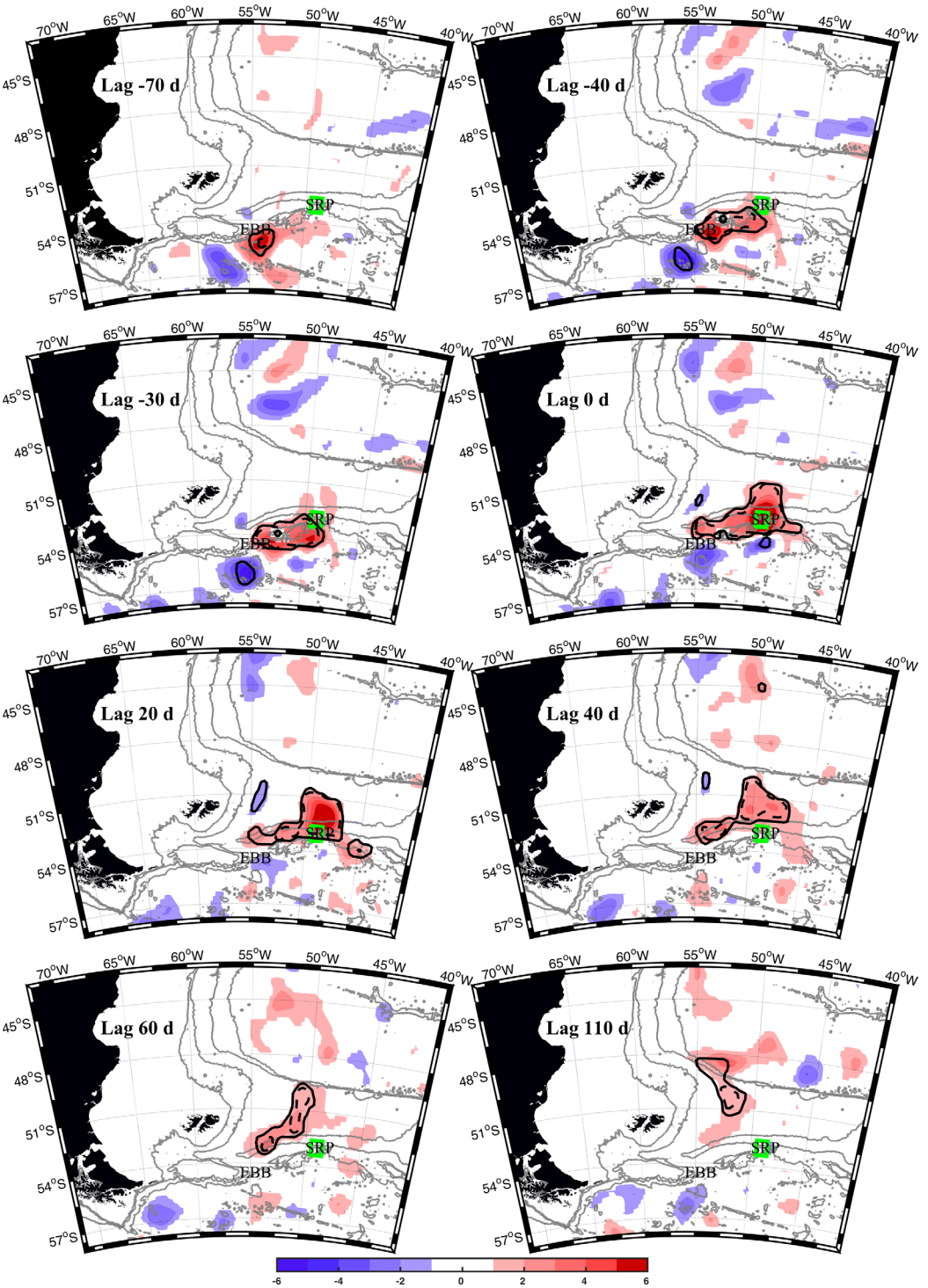

Figure 7. (continued)

The regression analysis is coherent with the EKE patterns (Figure 1c) described in the introduction: the local maximum south of the NSR corresponds to the increased anomalies as they are blocked by the topography, the EKE leaks northward through the EBB and SRP, and the preferred path for eddies over the Malvinas Trough and the central Malvinas Plateau is associated with the EKE values larger than 200 $cm^2\ s^{-2}$. Thus,

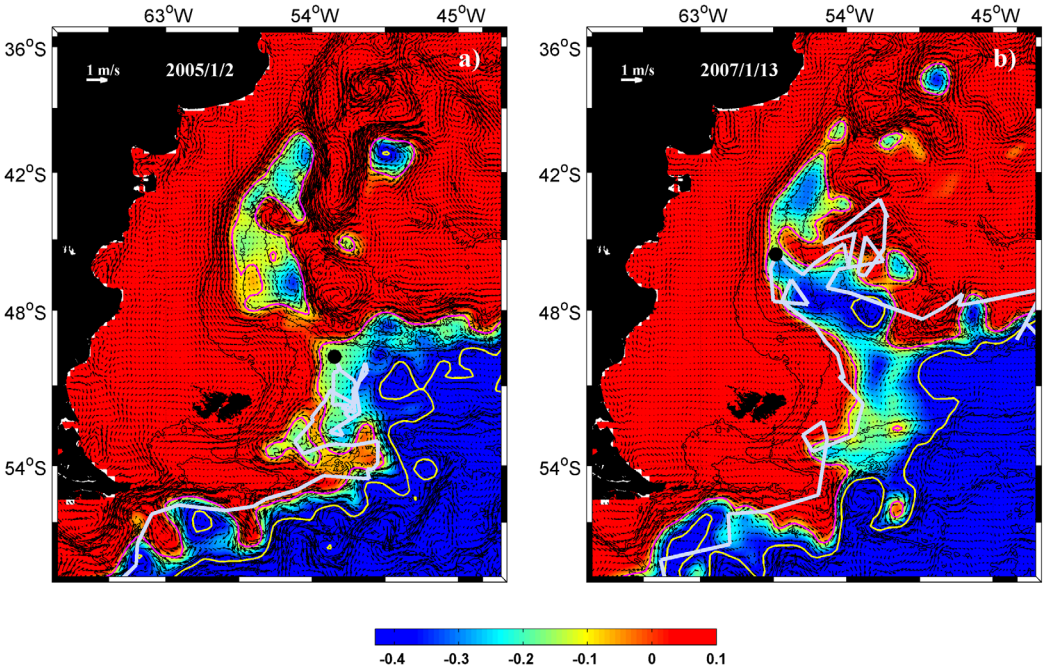

Figure 8. ADT fields (in m) corresponding to (a) 2 January 2005 and (b) 13 January 2007. Arrows correspond to the surface geostrophic velocities. The white lines represent the trajectory of Argo float 3900085 and 3900424. On each map, the black large dot indicates the position of Argo float at the corresponding date. The location of the SAF and PF are represented by red and yellow contours. Isobaths as in Figure 1a.

the Malvinas Plateau appears as a hot spot for dissipation and mixing. Consequently, flow variations associated with the SAF and PF observed at the SRP and EBB do not appear to impact the Malvinas Current, an exception being the coastal trapped waves proceeding from Drake Passage, which are only observed through the EBB.

3. Variations Along the Patagonian Continental Slope: Blocking Events

Among the selected Argo float trajectories (Figure 1d), two floats in the southern MC at 50°S did not reach latitudes lower than 49°S and 45°S, respectively, suggesting the occurrence of a recirculation or blocking phenomenon. These events are examined based on the ADT distributions.

3.1. Case Studies: Float 3900085 and Float 39000424

Argo float 3900085 (Figure 8a) crossed the NSR trough the SRP, then followed the 2000 m isobath to about 50°S and then recirculated southward. The ADT field and the surface geostrophic velocities corresponding to 2 January 2005, date of float 3900085 northernmost location, reveals a sharp eastward turn of the MC. This offshore flow is forced by a westward intrusion of relatively high ADT ($>$0.1 m) between 48 and 49.5°S which blocks the northward path of the MC. In this region, the ADT is significantly higher than the record length mean of $-$0.25 m. This blocking of the MC explains the path of the float.

In early January 2007, float 3900424 penetrates northward along the slope to about 45.5°S, where it describes a sharp offshore turn (Figure 8b). The ADT field corresponding to 13 January 2007 presents a westward intrusion of high ADT close to 45°S, which blocks the northward penetration of the MC beyond that latitude. Positive ADT values ($+$0.05 m) are found over the region 55°W–58°W and 46°S–45°S, a region characterized by significantly lower mean ADT ($-$0.25 m Figure 1b).

At the times of these blocking events, relatively intense cyclonic recirculation cells are observed further north. These recirculations are associated with ADT lower than $-$0.35 m at 55°W and 47°S in January 2005 (Figure 8a) and lower than $-$0.3 m at 56°W and 43°S in January 2007 (Figure 8b).

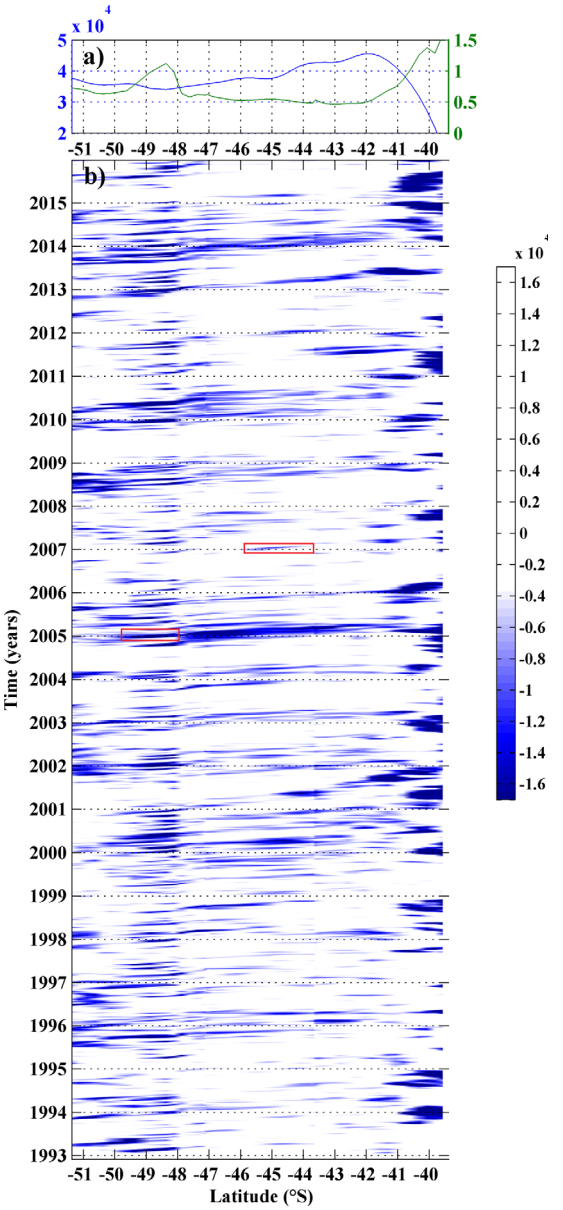

Figure 9. (a) Mean (blue line) and standard deviation (green line) of the surface transport of the Malvinas Current as a function of latitude in $m^2\ s^{-1}$. (b) Hovmöller diagram of the anomaly of the surface transport of the MC computed subtracting the mean from the altimetric period. The red boxes indicate the two events shown in Figure 8.

In the following section, we investigate whether these blocking events are exceptional or recurrent.

3.2. Recurrence of Blocking Events in the MC

To quantify the occurrence and location of blocking events along the Patagonian slope, we produced a time series of the surface transport (the transport per meter) of the MC. We computed the component of the AVISO surface geostrophic velocities across transects perpendicular to the bottom slope. The surface transport time series at each latitude was then calculated by integrating the surface velocity between the 1000 and 3000 m isobaths from 49°S to 39°S, and from the 1000 to 2500 m isobaths over the Malvinas Plateau from 51.5°S to 49°S. The mean surface transport is about $4 \times 10^4\ m^2\ s^{-1}$ which corresponds to an order of magnitude of 40 Sv with an equivalent-barotropic depth of 1000 m (60 Sv with 1500 m) (Figure 9a). The mean surface transport is maximum at 41.7°S and diminishes north of 41°S. The standard deviation of the surface transport is about four times smaller than the mean and shows two peaks: a large one associated with the Brazil-Malvinas Confluence north of 41°S and a peak of $1.3 \times 10^4\ m^2\ s^{-1}$ between 49°S and 48°S (Figure 9a). Only negative anomalies of the MC surface transport with an amplitude larger than $0.5 \times 10^4\ m^2\ s^{-1}$(the mean value of the standard deviation of the surface transport time series between 45°S and 42°S) are considered (Figure 9b).

Large negative values of the transport anomaly are recurrently found between 49°S and 48°S (Figure 9b). Some of these anomalies are just found in that latitudinal range, while others appear to propagate northward. The propagation velocity is rather uniform with estimated values of 0.12 m s^{-1} between 51°S and 48°S and 0.09 m s^{-1} north of 48°S. In some cases, for instance, at the beginning of 2010 and end of 2014, the negative anomalies came from south of 50°S (Figure 9b). However, most of the time, the negative anomalies are first seen between 49°S and 48°S. Some of them propagate northward and reach latitudes as low as 43°S. It is the case for the blocking event at the beginning of 2005 (shown in Figure 8a and indicated by a red box in Figure 9b). The Hovmöller diagram also shows several anomalies that do not propagate from the south, rather are first seen at latitudes lower than 48°S. For instance, the blocking event of 13 January 2007 (shown in Figure 8b and identified with a red box in Figure 9b) corresponds to an anomaly that shows up at 45°S for the first time on the Hovmöller diagram. Major anomalies to the north of 41°S are associated with intrusions of the BC, which, from time to time, reach latitudes as south as 41°S.

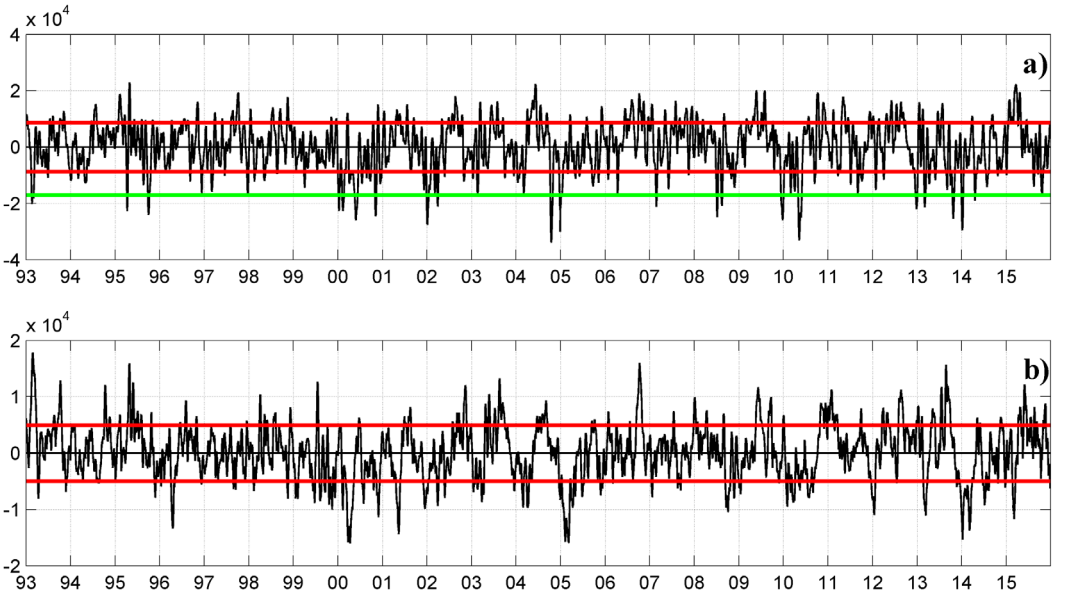

Figure 10. Time series of the MC surface transport anomalies (in $m^2\ s^{-1}$) computed over a box centered at (a) 48.5°S and (b) 44.5°S on the continental slope (the boxes are shown in red in Figure 11). The green line is the $-1.7 \times 10^4\ m^2\ s^{-1}$ values corresponding to a 50% decrease in surface transport and selects 26 blocking events.

Large negative surface transport anomalies do not show any clear periodicity or trend rather an irregular occurrence. Year 2005, for instance, presented negative anomaly values larger than $1.7 \times 10^4\ m^2\ s^{-1}$, corresponding to the blocking event shown in Figure 8a. Other years, like 2009, do not present significant negative anomalies in the surface transport.

3.3. Origin of the Blocking Events

Time series of the surface transport anomaly averaged over boxes centered at 44.5°S and 48.5°S (red boxes in Figure 11) are shown in Figure 10. The maximum correlation coefficient between the time series, 0.40 (>99% confidence limit), is obtained for a lag of 70 days, the surface transport time series at 48.5°S leading. To gain some insight into the origin of the blocking events, we produced lagged composite maps of SLA for the extreme cases corresponding to a reduction of the MC surface transport to 50% of the time averaged transport. This criterion identifies the 26 events with a negative surface transport anomaly larger than $1.7 \times 10^4\ m^2\ s^{-1}$ in amplitude in the 48.5°S times series (Figure 10a). Lagged composites of SLA for the times of the blocking events first detect a positive SLA around 48.5°S 48°W over the Argentine Abyssal Plain at lag −55 days (Figure 11). The positive SLA builds up at the same location, which corresponds to potential vorticity values between −1.76 and $-1.78 \times 10^{-8}\ m\ s^{-1}$, until lag −25 days, while a negative SLA to the north strengthens and a SLA dipole is observed over the Argentine Abyssal Plain (lags −35 and −25 days in Figure 11). The negative SLA appears to proceed from the north remaining over a potential vorticity plateau within the −1.72 to $-1.74 \times 10^{-8}\ m\ s^{-1}$ range. The SLA dipole builds up, moves south and anomalies spread in the zonal direction as they are blocked in the south by the Malvinas Escarpment (lags −15 and −5 days). The zonal potential vorticity contour associated with the Malvinas Escarpment is $-1.92 \times 10^{-8}\ m\ s^{-1}$. The positive SLA reaches 48.5°S 56°W (southern box) 55 days after its first detection. At that time, the positive SLA anomaly has an extension of 10° in longitude and 3° in latitude and an amplitude of 0.2 m (lag 0, Figure 11). It continues to propagate northwestward along the western slope of the Argentine Basin reaching 47.5°S (lag +10 days, Figure 11). At this point the $-1.92 \times 10^{-8}\ m\ s^{-1}$ potential vorticity contour changes orientation from zonal to north–northeast. The positive SLA splits in two parts (lags 20 and 30 days, Figure 11). One part propagates to the north along the western slope of the Argentine Basin along the 3000 m isobath, while the other one keeps following the $-1.92 \times 10^{-8}\ m\ s^{-1}$ contour to the northeast (lag 50 days). At lag 70 days, the positive SLA along the western slope of the Argentine Basin can be identified at the northern box (in agreement with the above mentioned maximum cross correlation) with a scaled-down amplitude (0.08 m). The positive SLA cannot be followed north of 44°S, as it is masked by the relatively intense variability associated with the Brazil-Malvinas Confluence.

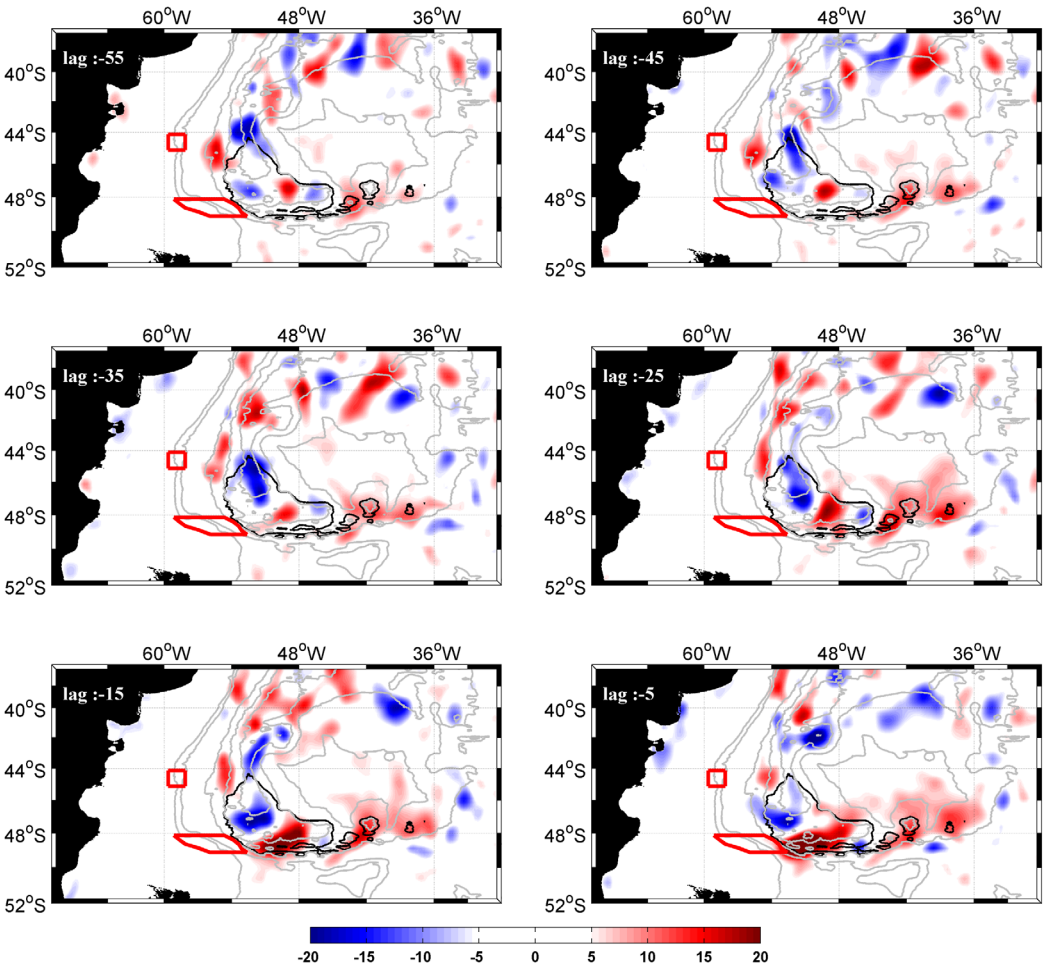

Figure 11. Lag composites of SLA for the 26 blocking events detected in the surface transport anomaly time series from Figure 10a. Color scale in centimeters. The time series anomalies presented in Figure 10 were computed over the red boxes centered at 48.5°S and 44.5°S. Grey isolines indicate the flowing potential vorticity contours (f/h): −6.00, −4.00, −1.92, −1.80, and -1.74×10^{-8} m s^{-1}.

The surface transport anomaly at the northern box never exceeds 1.7×10^4 m^2 s^{-1} in amplitude (Figure 10b), which means that at that location the surface transport is never reduced by 50%. We computed the lagged composites for the 29 events corresponding to a decrease of 35% of the surface transport in the northern box (amplitude larger than 1.2×10^4 m^2 s^{-1}, not shown). The patterns are similar to those shown in Figure 11 (with a lag increased by 70 days), the only difference being an intensification of the anomaly observed around 46°S at lag −20 days (i.e., lag +50 days in Figure 11) suggesting that local phenomena beyond the propagation of anomalies from the south affect the 35% decrease in surface transport in the northern box (Figure 8b is an example).

We conclude then that blocking events at 48.5°S are not directly associated with the crossing of the ACC over the NSR, but rather originate from positive SLA which build up over the deepest part of the Argentine Basin, propagate westward along the Malvinas Escarpment, and disconnect the MC from the ACC.

3.4. The MC Circulation During Blocking Events at 48.5°S

The 26 blocking events at 48.5°S with a 50% surface transport reduction last between 10 and 35 days, with a mean duration of 15 days (Figure 10a). Most blocking events occur in summer (12) or spring (10) and few in autumn (3) or winter (1) (none in June, August, and September).

The ADT composite map of the 26 blocking events (Figure 12a), corresponding to lag 0 anomaly composite distribution in Figure 11, shows high values of ADT (>-0.1 m) at 48.5°S 55°W where mean ADT values are −0.3 m (Figure 1b). It also presents a cyclonic circulation (ADT <-0.3 m) located at 47°S 55°W. These ADT

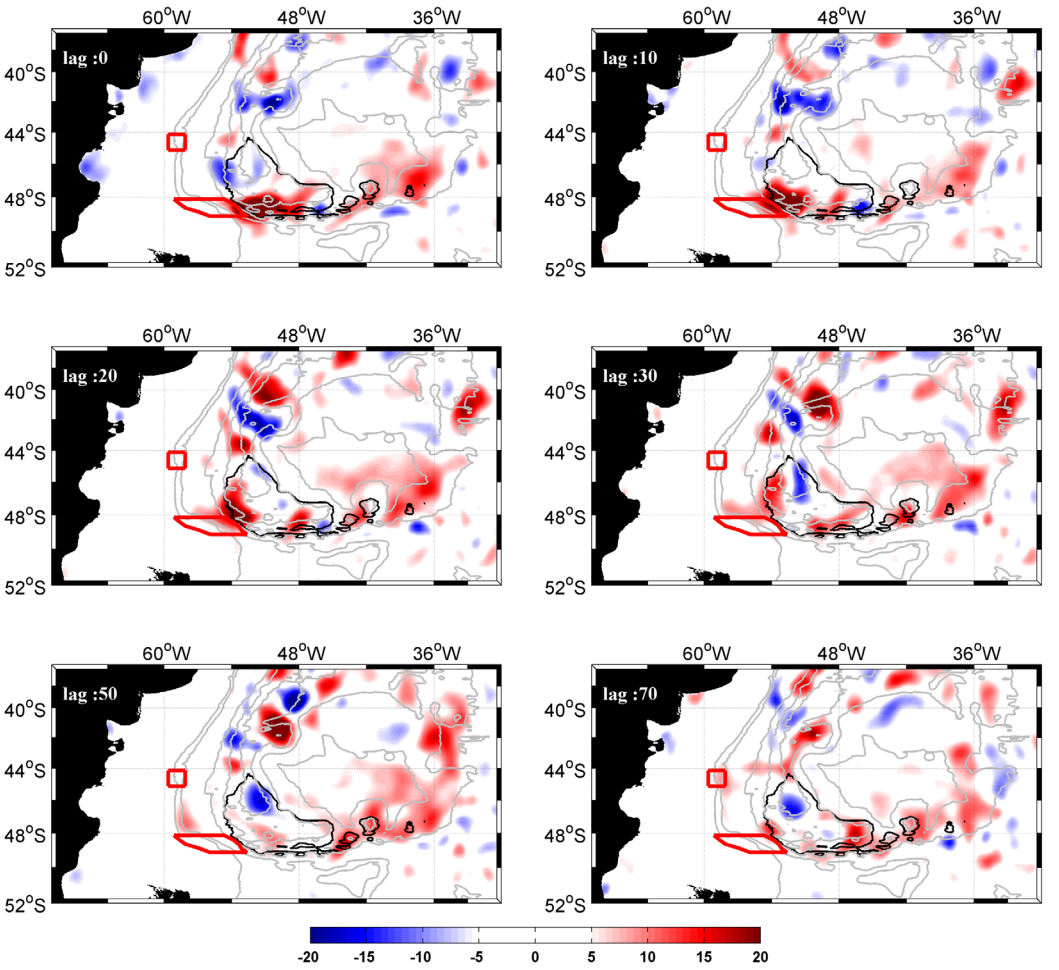

Figure 11. (continued)

values are reminiscent of the SLA dipole over the Argentine Abyssal Plain observed in the SLA lag composite (Figure 11). The ADT composite also shows that, at the surface, a large fraction of the northern MC is cut from its source. Nonetheless, the northern structure of the MC does not collapse: a cyclonic recirculation cell is established between 38°S and 48°S, with the MC as its western boundary and the northward penetration of the SAF still reaches ~40°S (as in Figure 1b), though the SAF itself is now disconnected from the circumpolar front, which has short-circuit the circulation and sharply veered eastward near 48°S. The ADT composite map does not reveal any intensification or reduction of the circulation of the Zapiola anticyclone and different situations can be observed during the years. During the period between 1999 and 2001 while the Zapiola transport was small [see *Saraceno and Provost*, 2012, Figure 8], four blocking events developed (Figure 10). On the other hand, during 2004 and 2005 when the Zapiola anticyclone transport is large, two strong (90% reduction in surface transport) and long-lasting (respectively, 22 and 23 days) blocking events are observed (Figure 10).

In fact, the 15 October 2004 event corresponds to the date of the absolute minimum in MC surface transport at 48.5°S: the transport is reduced by 99%. In contrast to the rather smooth ADT composite (Figure 12a), the ADT field in 15 October 2004 (Figure 12b) presents an exacerbated mesoscale field with numerous intense cyclones. The cyclonic eddy centered at 47°S 55°W, around the same location as the one in the ADT composite (Figure 12a), is stronger (ADT < -0.4 m) and appears to reinforce the obstruction of the MC (Figure 12b). The Brazil-Malvinas Confluence remains at 40°S and the full MC transport at 41°S [*Spadone and Provost*, 2009, Figure 12] shows values above its mean, probably associated with the intense, 150 km wide cyclonic eddy (centered at 41.5°S and 55°W) (Figure 12b). At the time of the largest blocking

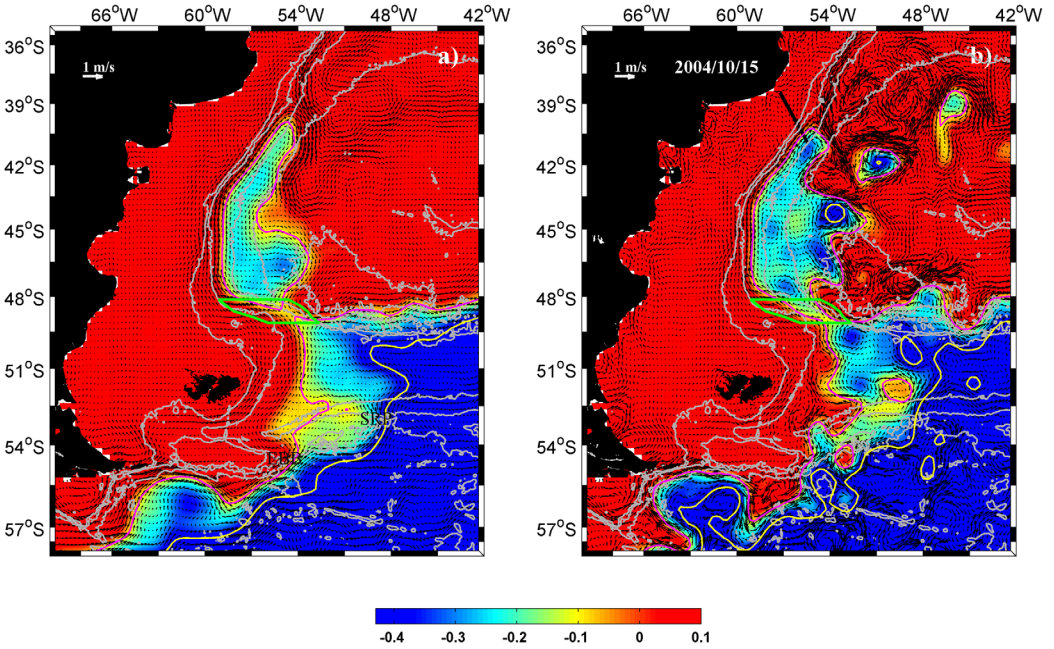

Figure 12. (a) Composite of ADT (in m) and surface geostrophic velocities (cm s^{-1}) of the 26 blocking events detected in the surface transport anomaly time series from Figure 10a (computed over the green box). (b) ADT field (in m) and surface geostrophic velocities (cm s^{-1}) corresponding to 15 October 2004. Black line shows the section across which the MC transport was calculated by *Spadone and Provost* [2009]. The location of the SAF and PF are represented by red and yellow contours. Isobaths as in Figure 1a.

event, the three cyclonic circulations observed along the slope at 47.5°S, 45°S, and 41.5°S contribute to maintaining a strong MC.

To summarize, we observed that although a large fraction of the MC is cut from its source during the blocking events, it does not collapse. Between 38°S and 48°S a robust cyclonic cell is established. The MC becomes the western boundary current of the cell and small cyclonic eddies locally reinforced the circulation.

4. Summary and Discussion

Argo floats and satellite altimetry provide valuable information on the MC circulation south of 41°S, a region lacking direct current observations. Argo float data reveal Antarctic Waters (south of the Polar Front waters) in the EBB and Subantarctic Waters (north of the SAF waters) in the SRP, indicating meandering of fronts or eddies through these passages. Satellite altimetry data were used to characterize the time-space variability of the SAF and PF through the NSR and the downstream impact of these variations. Variations associated with the SAF and PF at the SRP and EBB do not appear to impact the Malvinas Current further north, an exception being the coastal trapped waves proceeding from Drake Passage, which are only observed at the EBB. The Malvinas Plateau, where energetic deep-reaching eddies are trapped, follow preferential paths, break down, and vanish from altimetry maps, appears as a hot spot for dissipation and mixing. The spatial and temporal sampling of present satellite altimetry missions and the frequent cloud cover in the region impede a precise observation of eddies as they break and dissipate in either ADT maps or satellite infrared images. The precise fate of the small eddies remains unclear. Do they proceed northward or do they dissipate over the Malvinas Plateau? The exceptionally clear infrared image presented in section 2.3 (Figure 5h) shows that the large 100 km diameter eddy broke into two smaller eddies which are blurred in the corresponding ADT map (Figure 5g). At that period, first 2 weeks of August 2015, the MC surface transport at 48.5°S was reduced by 45% (Figure 10a) (note the elevated ADT values at 48.5°S and 52°W in Figure 5g). To the northwest of the two small eddies is seen another pair of small eddies which can be observed in ADT map a week before (Figure 5f). Is that pair trapped there because of the blocking or would it proceed to the north in other circumstances?

Peculiar Argo float trajectories, like the 3900085 and 3900424 (Figure 1d), pointed at blocking events of the MC. An analysis of 23 years of satellite sea surface height showed that blocking events at 48.5°S are a recurrent feature of the circulation of the MC. Over this period, we identified 26 blocking events during which the MC surface transport at 48.5°S was reduced by more than 50%. These intense blocking events last between 10 and 35 days, with a mean duration of 15 days. They preferentially occur in spring and summer, 12 were recorded during summer and 10 during spring, while only three were observed during autumn and only one during winter. Blocking events do not exhibit any significant trend in amplitude. The analysis suggests that these events originated from positive SLA anomalies that build up over the deepest part of the Argentine Basin (depth $>$ 6000 m) at around 48°W and 48.5°S and propagate westward along the Malvinas Escarpment reaching 55°W. Thus, intense blocking events are not directly associated with the crossing of the NSR by the ACC. Whether those blocking events are related to changes in the strength of the Zapiola anticyclone is unclear and was not carefully examined in the present study. The dynamical processes responsible for the generation of these blocking events have yet to be determined.

We used surface transport anomaly estimates as there are no direct observations of full MC transports at these latitudes. Full transports may behave somewhat differently, although the structure of the Malvinas Current has been shown to be close to barotropic-equivalent [*Vivier and Provost*, 1999a, 1999b]. This is why we cautiously focused on extreme negative events in the surface transport, which are most likely associated with minima in full transport, and did not examine the full surface transport variability.

Some of the lowest full-depth MC transports at 41°S [see *Spadone and Provost*, 2009] coincide with blocking events in the south: for example, the two long-lasting (30 days) minima with transports lower than 25 Sv observed in 2005 (their Figure 12) correspond with the upstream blocking events described above. The time lag between the blocking at 48°S and its signature at 41°S is about 120 days. However, the transport time series at 41°S is also significantly influenced by mesoscale activity from the Brazil-Malvinas Confluence and transport minima lower than 10 Sv in 1994 and 2001 [*Spadone and Provost*, 2009, Figure 12] are clearly of Brazil-Malvinas Confluence origin (Figure 9b). Other blocking events that caused significant drops in the surface transport in 1994 and 2001 (Figure 9b) did not propagate northward and were not observed at 41°S.

Our analyses suggest that mesoscale eddies from the southern Argentine Basin are responsible for a large fraction of the variability of the MC transport observed north of about 48.5°S. This may explain why the northward penetrations of the MC are uncoupled from the ACC variability, as suggested by observations [*Garzoli and Giulivi*, 1994] and numerical models [*Fetter and Matano*, 2008]. New current-meter data are being acquired at two sites of the MC (41°S and 45°S) (http://www.cima.fcen.uba.ar/malvinascurrent/en/). They will be used to produce transport time series of the MC. The whole range of full-depth transport variations, not only extreme events, will then be examined.

Further work is needed to investigate the circulation and mixing processes over the Malvinas Plateau which appear to efficiently damp the variability coming from Drake Passage except for the coastal-trapped waves and to understand the dynamical processes responsible for blocking events. To better document the circulation and eddy evolution over the Malvinas Plateau, regional altimetric gridded maps with a higher spatial resolution are being produced and analyzed in collaboration with CLS Argos (Collect Localisation Satellites). High-resolution (1/12°) operational models with assimilation of satellite altimetry data and Argo float data reproduce a realistic meridional extension of the MC and blocking events. Analyses of outputs of such models could give some insight into the processes responsible for the blocking at 48.5°S.

Acknowledgments
The altimeter products were produced by Ssalto/*Duacs* and distributed by *Aviso*, with support from *CNES* (http://www.aviso.altimetry.fr/duacs/). The float data were collected and made freely available by the International Argo Program and the national programs that contribute to it (http://www.argo.ucsd.edu,// argo.jcommops.org). The Argo Program is part of the Global Ocean Observing System. The authors are deeply grateful to the CNES (Centre National d'Etudes Spatiales) for the strong and constant support. This study is a contribution to EUMETSAT/CNES DSP/OT/12-2118. We acknowledge support from the MINCYT-ECOS-Sud A14U0 projects ECOS-Sud program in facilitating scientific exchanges between Argentina and France. Camila Artana and Zoe Koenig are funded under PhD scholarships from Université Pierre et Marie Curie.

References

Barré, N., C. Provost, A. Renault, and N. Sennéchael (2011), Fronts, meanders and eddies in Drake Passage during the ANT-XXIII/3 cruise in January–February 2006: A satellite perspective, *Deep Sea Res., Part II, Topical Studies in Oceanography*, *58*(25), 2533–2554, doi:10.1016/j.dsr2.2011.01.003.

Chelton, D. B., M. G. Schlax, D. L. Witter, and J. G. Richman (1990), Geosat altimeter observations of the surface circulation of the Southern Ocean, *J. Geophys. Res.*, *95*, 17,877–17,903, doi:10.1029/JC095iC10p17877.

Fetter, A. F. H., and R. P. Matano (2008), On the origins of the variability of the Malvinas Current in a global, eddy-permitting numerical simulation, *J. Geophys. Res.*, *113*, C11018, doi:10.1029/2008JC004875.

Fu, L. L. (2006), Pathways of eddies in the South Atlantic Ocean revealed from satellite altimeter observations, *Geophys. Res. Lett.*, *33*, L14610, doi:10.1029/2006GL026245.

Garzoli, S. L., and C. Giulivi (1994), What forces the variability of the Southwestern Atlantic Boundary Currents?, *Deep Sea Res., Part I*, *41*, 1527–1550.

Gordon, A. L. (1989), Brazil Malvinas Confluence-1984, *Deep Sea Res., Part I*, *36*(3), 359–384, doi:10.1016/0198-0149(89)90042-3.

Koenig. Z., C. Provost, Y.-H. Park, R. Ferrari, and N. Sennéchael (2016), Anatomy of the Antarctic Current volume transport through Drake Passage, *J. Geophys. Res. Oceans*, *121*, 2572–2595, doi:10.1002/2015JC011436.

Nowlin, W. D., Jr., T. Whitworth III, and R. D. Pillsbury (1977), Structure and transport of the Antarctic Circumpolar Current at Drake Passage from short-term measurements, *J. Phys. Oceanogr.*, *7*(6), 788–802.

Orsi, A. H., I. T. Whitworth, and J. W. Nowlin (1995), On the meridional extent and fronts of the Antarctic Circumpolar Current, *Deep Sea Res., Part I*, *42*, 641–673, doi:10.1016/0967-0637(95)00021-W.

Piola, A. R., and A. L. Gordon (1989), Intermediate Waters in the Southwest South-Atlantic, *Deep Sea Res., Part I*, *36*(1), 1–16, doi:10.1016/0198-0149(89)90015-0.

Provost, C., A. Renault, N. Barré, N. Sennéchael, V. Garçon, J. Sudre, and O. Huhn (2011), Two repeat crossings of Drake Passage in austral summer 2006: Short-term variations and evidence for considerable ventilation of intermediate and deep waters, *Deep Sea Res., Part II*, *58*(25), 2555–2571, doi:10.1016/j.dsr2.2011.06.009.

Saraceno, M., and C. Provost (2012), On eddy polarity distribution in the southwestern Atlantic, *Deep Sea Res., Part I*, *69*, 62–69, doi:10.1016/j.dsr.2012.07.005.

Saraceno, M., C. Provost, A. R. Piola, J. Bava, and A. Gagliardini (2004), The Brazil Malvinas Frontal System as seen from nine years of AVHRR data, *J. Geophys. Res.*, *109*, C05027, doi:10.1029/2003JC002127.

Saraceno, M., C. Provost, and U. Zajackovski (2009), Long-term variation in the anticyclonic ocean circulation over the Zapiola Rise as observed by satellite altimetry: Evidence of possible collapses, *Deep Sea Res., Part I*, *56*, 1077–1092, doi:10.1016/j.dsr.2009.03.0005.

Saunders, P. M., and B. A. King (1995), Bottom current derived from a shipborne ADCP on WOCE cruise A11 in the South Atlantic, *J. Phys. Oceanogr.*, *25*, 329–347.

Smith, W. H. F., and D. T. Sandwell (1994), Bathymetric prediction from dense satellite altimetry and sparse shipboard bathymetry, *J. Geophys. Res.*, *99*, 21,803–21,824.

Sokolov, S., and S. R. Rintoul (2009a), The circumpolar structure and distribution of the Antarctic Circumpolar Current fronts. Part 1: Mean circumpolar paths, *J. Geophys. Res.*, *114*, C11018, doi:10.1029/2008JC005108.

Sokolov, S., and S. R. Rintoul (2009b), Circumpolar structure and distribution of the Antarctic Circumpolar Current fronts: 2. Variability and relationship to sea surface height, *J. Geophys. Res.*, *114*, C11019, doi:10.1029/2008JC005248.

Spadone, A., and C. Provost (2009), Variations in the Malvinas Current volume transport since October 1992, *J. Geophys. Res.*, *114*, C02002, doi:10.1029/2008JC004882.

Vivier, F., and C. Provost (1999a), Direct velocity measurements in the Malvinas Current, *J. Geophys. Res.*, *104*, 21,083–21,103, doi:10.1029/1999JC900163.

Vivier, F., and C. Provost (1999b), Volume transport of the Malvinas Current: Can the flow be monitored by TOPEX/Poseidon?, *J. Geophys. Res.*, *104*, 21,105–21,122, doi:10.1029/1999JC900056.

Vivier, F., C. Provost, and M. Meredith (2001), Remote and local forcing in the Brazil Malvinas Region, *J. Phys. Oceanogr.*, *31*, 892–913, doi:10.1175/1520-0485.

Volkov, D. L., and L. L. Fu (2008), The role of vorticity fluxes in the dynamics of the Zapiola Anticyclone, *J. Geophys. Res.*, *113*, C11015, doi:10.1029/2008JC004841.